Optical properties of HgTe/CdTe superlattices in the normal, semimetallic, and inverted-band regimes

Z. Yang,* Z. Yu, Y. Lansari, S. Hwang, J. W. Cook, Jr., and J. F. Schetzina
Department of Physics, North Carolina State University, Raleigh, North Carolina 27695-8202
(Received 7 June 1993)

The optical properties of HgTe/CdTe superlattices (SL's) in the three principal regimes are summarized. Experimental results from the photoluminescence and the cyclotron resonance of electrons and holes both parallel and perpendicular to the SL layer plane in the SL's in the normal semiconducting regime are presented. These results, together with the previously reported optical and magneto-optical spectra of a series of SL's in the inverted-band regime, are analyzed systematically under the framework of a six-band $\mathbf{k}\cdot\mathbf{p}$ model. Using a single value of 550 meV for the valence-band offset (VBO) the model correctly predicts all the major experimental results. These include (i) the energy gap between the electron subband and the heavy-hole subband and the energy gap between the electron subband and the light-hole subband of the SL's in the normal regime over the temperature range from 4.5 to 150 K, (ii) the in-plane masses of the electrons and holes and the Voigt geometry mass of electrons of the SL's in the normal semiconducting regime, (iii) the in-plane electron and hole masses in a SL in the semimetallic regime, (iv) the energy gap between the second electron subband and the second heavy-hole subband in the SL's in the inverted-band regime, and (v) the electron in-plane masses of the SL's in the inverted-band regime. The value of VBO that fits the experimental results is 550±50 meV at 5 K and it reduces, probably linearly, to 500±50 meV at 120 K. The origin of the discrepancy between the value of VBO found in this work and the ones reported in earlier works is discussed.

I. INTRODUCTION

The HgTe/CdTe superlattices (SL's) have been extensively investigated since they were proposed by Schulman and McGill[1] in 1979 as a material for infrared detectors and other optoelectronic applications in the 3- to 12-μm spectrum region. They belong to a class of SL's, namely, the type-III SL's, because of the unique combination of a negative band-gap semiconductor HgTe and a positive band-gap semiconductor CdTe. With controlled HgTe and CdTe layer thicknesses, the band gap of the SL can be tailored to a desired value anywhere from zero to a few hundred meV, covering the whole 3- to 12-μm spectrum region.

It has recently been established[2,3] that HgTe/CdTe SL's exist in one of three principal regimes, namely, the normal regime, the semimetallic regime, and the inverted-band regime, depending mainly on the HgTe quantum-well layer thickness L_z. SL's in different regimes have markedly different properties. In a SL with thin HgTe wells (<70 Å) the first electron subband $E1$ is above the first heavy-hole subband $H1$, the $E1$ subband being the first conduction subband and the $H1$ subband being the first valence subband, as shown in Fig. 1(a). These thin-well SL's with positive band gaps are in the normal regime. As the HgTe well width increases, the $E1$ subband moves towards the $H1$ subband until the two subbands cross each other at a certain k_z point [Fig. 1(b)], where k_z, is the wave vector of the electrons perpendicular to the SL layers. In the k_z region where the $E1$ subband is below the $H1$ subband, the first valence subband is the $E1$ subband and the first conduction subband is the $H1$ subband, while in the k_z region where the $E1$ subband is above the $H1$ subband, the first valence subband is the $H1$ subband and the first conduction subband is the $E1$ subband. The SL's with this type of subband structure are in the semimetallic regime. As the HgTe well width further increases, the $E1$ subband moves further down and a small negative gap appears between $E1$ and $H1$. The SL's are in the inverted-band regime since now the $H1$ subband serves as the first conduction subband and the $E1$ subband serves as the first valence subband.[2] The

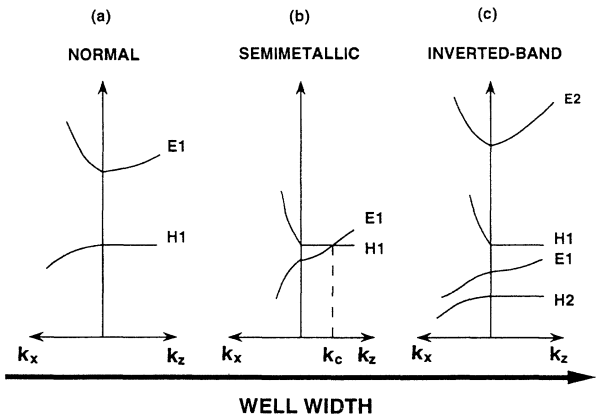

FIG. 1. Subband structure of HgTe/CdTe superlattices in (a) the normal semiconducting regime, (b) the semimetallic regime, and (c) the inverted-band regime. The $E1$ and $H1$ subbands cross each other at the point where $k_z=k_c$ in the semimetallic regime.

second heavy-hole subband $H2$ may move above the $E1$ subband as the well width increases even further and replace the $E1$ subband as the first valence subband of the SL. For SL's with thick barriers (>45 Å), the $E1$ subband is almost flat along the k_z direction. The crossing of the $E1$ and the $H1$ subbands, therefore, does not take place and such SL's, which are often called multiple quantum wells (MQW's), exist in only one of the two principal regimes, namely, the normal regime and the inverted-band regime.

The optical properties of the SL's in the normal semiconducting regime have been extensively studied. Infrared (IR) absorption spectra and photoluminescence (PL) of a number of the SL's were measured.[4-8] The PL peak position shifted to higher photon energy as the temperature was raised,[4,5] while the origin of the PL was not clearly known. Steplike features of the absorption spectra were observed[6] that manifest the unique characteristics of the quantum confinement of the electronic states in SL's. The split between the first light-hole subband $L1$ and the first heavy-hole subband $H1$ was identified[6,7] and was later studied at different temperatures.[8] The $L1$ and $H1$ subband split was also observed in HgCdTe/CdTe SL's.[9]

One of the most controversial issues since the beginning of the research on HgTe/CdTe SL's has been the value of the valence-band offset (VBO) between HgTe and CdTe when the two materials are grown epitaxially one on top of the other. Early far-infrared (FIR) magneto-optical experiments indicated that the value of VBO was small (~ 40 meV).[10-12] However, these results might have a large error because of the uncertainty in determining the thickness and the degree of the interdiffusion in the well and barrier layers. The energy position of the absorption feature due to the electron optical transition from the $L1$ subband to the $E1$ subband which was consistently observed in almost all the HgTe/CdTe SL's studied in this and others laboratories[6,9] indicated that the $H1$-$L1$ gap was larger than 100 meV in the semiconducting SL's. Further analysis using a six-band $\mathbf{k}\cdot\mathbf{p}$ model showed that the model could fit the measured $E1$-$H1$ gap and the $E1$-$L1$ gap at temperatures from 5 to 205 K when a value of 400 meV for VBO was used,[8] an error margin of ± 70 meV for VBO being estimated from the optical spectra without considering the possible thickness deviation of the layers in the SL's from their nominal values. Further experimental evidence which supports a large VBO (~ 400 meV) came from the measurement of the electron effective-mass anisotropy[13] and from the recent discovery that in the SL's in the inverted-band regime, the electron effective mass parallel to the SL layers *increases* as the HgTe well layer width *increases*.[3] A VBO of the order of 400 meV is consistent with the x-ray-photoemission experiment.[14]

In this paper, we report a complete study of the electronic subband characteristics of HgTe/CdTe SL's obtained from the optical and magneto-optical study of a large number of HgTe/CdTe SL's in all three regimes. First, we will report the IR absorption and PL experiments carried out over a wide range of temperatures for the SL's in the normal semiconducting regime. The origins of the PL peaks were identified by comparing their peak energy position with the absorption spectra measured at the same temperature, by the temperature dependence of their peak positions and intensities, and by the dependence on the laser pumping power of the peak intensities. Photoluminescence due to a variety of electron-hole recombination processes was observed. The $E1$-to-$H1$ direct recombination was routinely observed in most of the semiconducting SL's, and for the first time the $E1$-to-$L1$ direct recombination was observed in two SL's. The observed sharp and strong PL peaks made it possible to determine the $E1$-$H1$ and $E1$-$L1$ band gaps more precisely than ever before. The recombination of both the $E1$-$H1$ and the $E1$-$L1$ electron-hole pairs bound to impurity states was observed in intentionally doped SL's. PL peaks distinctively different from the above-mentioned ones were observed in SL's with high defect concentrations. We will then report the results of far-infrared magnetotransmission of the semiconducting SL's measured in a variety of geometries and polarizations. Cyclotron motions parallel to the SL layers of both electrons and holes, the cyclotron motion of electrons perpendicular to the layers, and absorption due to electronic transitions between the energy levels of shallow donors were observed. The IR absorption and FIR magnetotransmission spectra of a semimetallic SL will also be reported. Finally, the results of the above-mentioned experiments, together with the previous reported results for the inverted-band SL's[3] and semiconducting SL's,[8] were analyzed within the framework of the six-band $\mathbf{k}\cdot\mathbf{p}$ model, taking into account the possibility of the deviation of the actual layer thicknesses from the nominal ones estimated from the growth parameters. It was hoped that by comparing the theoretical results with a large amount of experimental data obtained from several different experiments on the SL's with a wide range of HgTe layer widths from 32 Å (in the semiconducting regime) to 158 Å (in the inverted-band regime), we would be able to establish the legitimacy of the $\mathbf{k}\cdot\mathbf{p}$ model for the HgTe/CdTe superlattices and obtain a reliable value for the valence-band offset between HgTe and CdTe.

The rest of the paper is divided into the following sections: In Sec. II the SL sample preparation and the experimental methods are briefly described. The $\mathbf{k}\cdot\mathbf{p}$ model is presented in Sec. III. In Sec. IV we present the experimental results and the analysis, followed by discussions about the value of VBO in Sec. V and conclusions in Sec. VI.

II. EXPERIMENTS

The SL's presented in this paper were all grown in this laboratory on either (100) or (211)B lattice-matched CdZnTe or CdTe substrates at temperatures from 120 °C to 170 °C by photoassisted molecular-beam epitaxy, except for the superlattices SLCT617, SLCT619, and SLCT632, which were grown on (211)B CdTe substrates at 170 °C by the same growth technique at General Electric Electronics Laboratory. Dopants were introduced only during the growth of the barrier layers for intentional modulation doping. There were at least 200 double

layers in each SL. The CdTe barrier layers of the SL's contained about 15% of Hg because of the presence of the Hg over pressure during the growth of the barrier layers. Theoretical results, however, showed that the effect of this small amount of Hg in the barrier layer on the subband structures was negligibly small, except for the subband dispersion perpendicular to the layers. The double-layer thickness of the barrier and well of each SL was obtained by dividing the measured total thickness of the SL by the number of periods, and by the angular spacing of the satellite peaks of the x-ray double-crystal diffraction. The ratio of barrier thickness to well thickness of most of the SL's was estimated from the growth parameters, while a small portion of the SL's were examined using transmission electron microscopy (TEM).

IR absorption and PL of the SL's were measured with a Nicolet 60SXR Fourier-transform IR spectrometer specially set up for double-modulation operation in the spectral range from 2 to 14 μm and at temperatures from 4.2 to 300 K. A cw Nd:YAG (where YAG denotes yttrium aluminum garnet) laser was used as excitation for the PL experiment, and the pump intensity on the sample was varied from 6.4 to 800 mW/cm^2 with a set of neutral density filters. A glowbar was used as the IR light source in the absorption experiment. Both the laser beam and the IR source were modulated at 3.5 KHz by a mechanical chopper. The scan speed of the spectrometer was set slow enough so as to match the response time of the lock-in amplifier.

Far-infrared magneto-optical experiments were carried out in the spectral range from 96.5 to 495 μm, in magnetic fields up to 7 T, and at temperatures from 4.2 to 200 K. An Apollo Model 122 FIR laser was used to illuminate the SL at normal incidence. The magnetic field was applied either perpendicular to (Faraday geometry) or parallel to (Voigt geometry) the SL layers. In the Faraday geometry the incident FIR beam was circularly polarized so that the electron cyclotron resonance (ECR) could be distinguished from the hole cyclotron resonance (HCR). The laser beam was linearly polarized perpendicular to the magnetic field in the Voigt geometry and both the ECR and HCR were excited. The samples were placed in a Janis split-coil superconducting magnet cryostat equipped with crystal quartz FIR windows. A silicon bolometer was used to detect the FIR radiation transmitted through the sample, and a second silicon bolometer was used to detect a portion of the incident FIR beam reflected from a beam splitter in front of the sample. The ratio of the transmission through the sample over the reflection from the beam splitter was then recorded as a function of the magnetic field.

Hall effect measurements were performed at temperatures from 4.2 to 300 K and at several magnetic fields up to 2 T. The Hall coefficient and mobility at each magnetic field were obtained by the standard Van der Paul method. Mobility-spectrum analysis was performed on the magnetic-field-dependent Hall data to obtain the concentration and mobility of each carrier species in the SL's. The results were reconfirmed by using a nonlinear least-squares fit once the number of species was known from mobility-spectrum analysis.

III. THEORETICAL MODEL

The six-band $\mathbf{k}\cdot\mathbf{p}$ SL model used in this investigation is essentially the same as the model proposed by Smith and Mailhiot.[15] First, the wave function of the SL was expended in terms of the linear combination of the bulk wave functions of each constituent. For HgTe and CdTe the bulk wave functions were obtained by solving a 6×6 Hamiltonian matrix which includes the two Γ_6 and the four Γ_8 bands. The spin split-off Γ_7 bands were treated as remote bands because they are about 1 eV away from the SL valence and conduction subbands. The Luttinger parameters were changed accordingly. The boundary conditions[16] were then imposed on the SL wave function at each interface and the big imaginary k values of the bulk wave function were limited to a certain value in order not to cause numerical problems in the computation.[16] The bulk-band parameters used in the calculation before the Γ_7 band correction were $E_p=19\,500$ meV, $\gamma_1=3.3$, $\gamma_2=-0.5$, $\gamma_3=0.67$, $\kappa=-1.3$, and $\Delta=1.0$ eV for HgTe, and $E_p=18\,000$ meV, $\gamma_1=1.54$, $\gamma_2=0.015$, $\gamma_3=0.133$, $\kappa=-0.605$, and $\Delta=0.977$ eV for CdTe. All the parameters except for the band gaps were assumed to depend linearly on the composition in the case of $Hg_{1-x}Cd_xTe$ alloy and are temperature independent. The composition and temperature dependences of the band gap of $Hg_{1-x}Cd_xTe$ alloy were taken from Ref. 17. The valence-band offset between HgTe and $Hg_{0.15}Cd_{0.85}Te$ was used as a fitting parameter. The well and barrier layer thicknesses were allowed to vary within a few monolayers (ML's) of the value estimated from the growth rates.

IV. RESULTS AND ANALYSIS

The experimental results of the SL's are presented below in accordance with the regimes to which they belong.

A. Normal regime

Infrared absorption spectra were measured for all the SL's at temperatures from 5 to 200 K. The $E1$-$H1$ band edge and the $E1$-$L1$ band edge were clearly manifested in all the spectra. Photoluminescence was observed in most of the SL's. The origins of the PL were identified by comparing the PL spectra with the IR absorption spectra at different temperatures, and by studying the temperature dependence of the intensity of the PL. The origins found were the direct recombination between the $E1$-$H1$ electron-hole pairs and between the $E1$-$L1$ electron-hole pairs, and the impurities and/or defect-related recombination.

1. PL at the E1-H1 band edge

The PL due to the $E1$-$H1$ electron-hole recombination was observed in most of the SL's. Figure 2 shows a typical PL spectrum (solid curve) along with the absorption spectrum obtained at the same temperature (dashed curve) for sample SLCT617. The sharp PL peak coincided with the first steep edge at 130 meV of the absorption spectrum, and the two features moved together towards

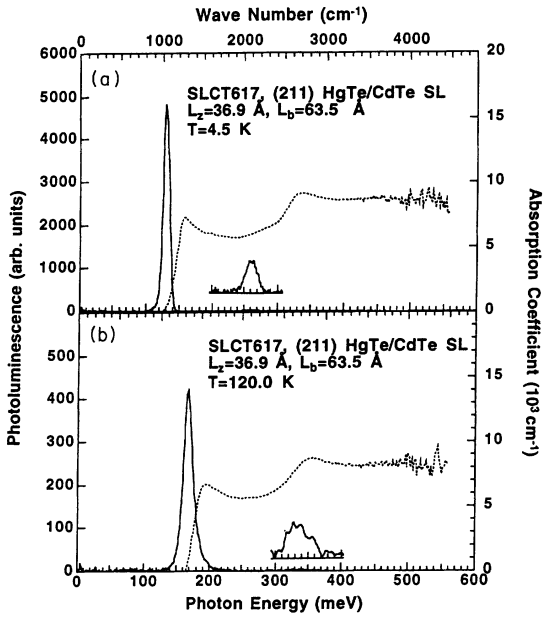

FIG. 2. The photoluminescence (solid curve) and the absorption spectra (dashed curve) of superlattice SLCT617 in the normal semiconducting regime with well width $L_z = 36.9$ Å and barrier width $L_b = 63.5$ Å at (a) 4.5 K and (b) 120 K. The insertions show the magnified PL peaks near the $E1$-$L1$ band edge. The noise on the high-energy side was due to the low intensity of the light source in the spectral region.

higher photon energy at higher temperatures. The absorption edge was due to the electronic transition from the $H1$ subband to the $E1$ subband, and the PL was due to the $E1$-$H1$ electron-hole pair recombination. The intensity of the PL peak changed linearly with laser pumping power until it reached 160 mW/cm^2 when it started to show signs of saturation and decreased monotonically as the temperature was raised. The typical drop in intensity was about a factor of 10 when the temperature was changed from 4.5 to 80 K.

The experimental $E1$-$H1$ band gaps of the SL's determined from the PL peaks and the absorption edges as a function of temperature were compared with theory. Figure 3 shows the theoretical band gap as a function of temperature for VBO=550 and 500 meV (two dashed curves) along with the experimental band gap (points) for samples SLCT617, SLCT632, and A121. The band gaps of these SL's were obtained from their PL spectra and the error margins were taken as one quarter of the full width at half height of the PL peaks. It is seen that the experimental points fall within the two theoretical curves, and the experimental band gap is close to the VBO=550 meV curve at 5 K and is close to the VBO=500 meV curve at 120 K. This indicates that the VBO changes slowly from 550 meV at 5 K to 500 meV at 120 K. The theoretical band gap obtained by assuming a linear dependence of VBO on temperature is shown as a solid curve in the same figure. It is seen that this theoretical curve fits very well the measured band gaps.

2. PL at the E1-L1 band edge

The insert in Fig. 2 shows a well-defined PL peak near the second absorption edge due to the electronic transition from the $L1$ subband to the $E1$ subband, and is therefore believed to be due to the $E1$-$L1$ electron-hole recombination. This absorption edge rises much more slowly than the $E1$-$H1$ band edge because of the light mass of the light-hole subband both parallel and perpendicular to the layers. Both the edge and the PL peak moved to higher photon energy at higher temperature, the PL peak moving faster than the edge, as can be seen by comparing the relative position of the PL peak and the edge at 5 and 120 K. The thermal distribution of photocarriers on the $L1$ subband was probably the cause for

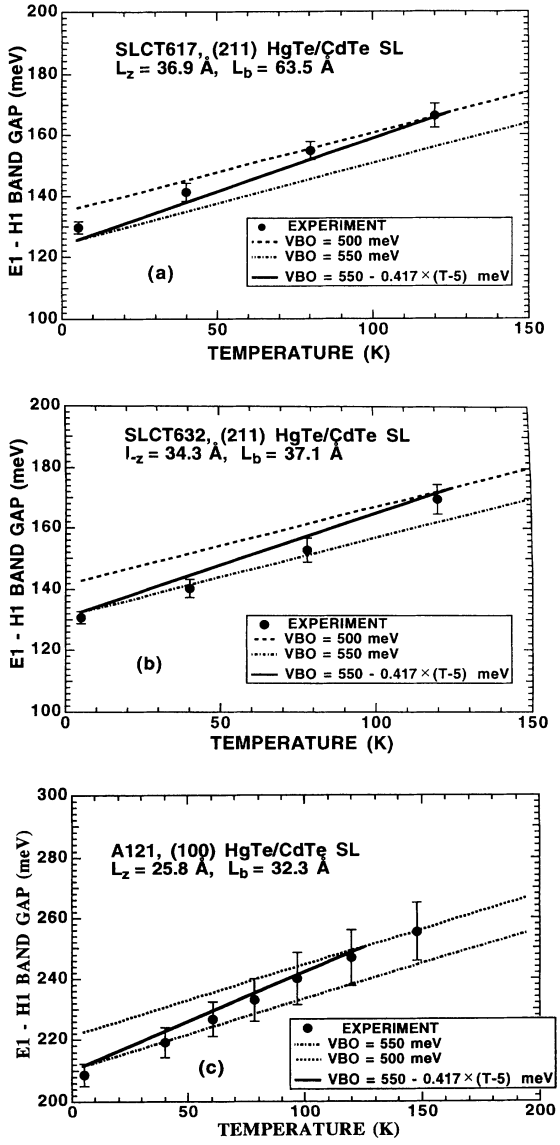

FIG. 3. Experimental band gap (points) versus temperature and the theoretical band gap using the valence-band offset =550 and 500 meV (two dashed line) for (a) superlattice SLCT617, (b) superlattice SLCT632, and (c) superlattice A121. The solid curve represents the theoretical band gap when a linear temperature dependence of the VBO is used.

the PL peak to be at higher energy than the $E1$-$L1$ band edge at higher temperatures.

3. Temperature dependence of the E1-H1 and E1-L1 band gaps

The $E1$-$H1$ and the $E1$-$L1$ band gaps of the other SL's in which the corresponding PL peaks were not observed were obtained from the energy positions of the edges of their IR absorption spectra. Listed in Tables I and II are the experimental band gaps at different temperatures along with the theoretical values for all the SL's in the normal regime. The same temperature-dependent VBO was used, although both the values of 550 and 500 meV for VBO could be used since the band gaps obtained from the absorption spectra carried a much larger error margin than the ones obtained from the PL spectra. The $E1$-$L1$ band gaps at temperatures higher than 5 K were determined from the absorption spectra even if the PL peaks were observed, because it is observed that the PL peaks moved faster than the edge, as has been described in Sec. IV A 2. The well and barrier thicknesses used in the calculation for each SL are listed along with the corresponding values estimated from the growth parameters (in parentheses), which differ up to 1 ML for the (100)-oriented SL's and up to 2 ML's for the (211)-oriented SL's, except for sample A90B which was the first (211) SL grown in this laboratory. The theoretical band gaps agree well with the experimental ones at all temperature except in the cases of the $E1$-$L1$ gap at 5 K for SLCT617 and A90B, and the $E1$-$H1$ gap at 120 K for SLCT619.

4. Impurity- and defect-related PL

Figure 4 shows the PL and absorption spectra of sample SLCT632 which was modulation doped with As. The strong PL peak at the $E1$-$H1$ band edge was due to the $E1$-$H1$ recombination, while the second PL peak at lower photon energy was believed to be due to the $E1$-$H1$ exciton bound to the As acceptor. Both the Hall measurement and the FIR magneto-optical experiment show that the SL was p type, as will be presented in Secs. IV A 5–IV A 7. The low-energy peak moved to higher photon energy as the temperature was raised, but not as fast as the $E1$-$H1$ band-edge peak. A linear relation was found between the pumping power and the intensities of both PL peaks. The intensities decrease as the temperature was raised and the relative intensity of the two peaks remained the same. The insert of Fig. 4 shows the PL peaks near the $E1$-$L1$ band edge. The peak at the $E1$-$L1$ band edge was the $E1$-$L1$ recombination and the lower-

TABLE I. The list of experimental and theoretical $E1$-$H1$ and $E1$-$L1$ gaps at various temperatures for superlattices in the normal semiconducting regime grown on the (100) crystal surface. The well and barrier thicknesses used in the calculation are also listed for each sample. The values of the thicknesses in the parentheses are the estimates from the growth parameters.

Sample (Orientation)	L_z(Å)/L_b(Å)	$E1$-$H1$ gap (meV) Experiment	$E1$-$H1$ gap (meV) Theory	$E1$-$L1$ gap (meV) Experiment	$E1$-$L1$ gap (meV) Theory	Temperature (K)
		208.5±4	211.12	331.8±15	349.28	5.0
A121	25.8/32.3	219.0±5	222.00	337.5±15	357.26	40.0
(100)	(25.8/35.5)	232.9±9	234.43	352.7±20	366.76	80
		246.9±9	246.86	358.6±20	375.51	120
		146.4±5	145.63	278.1±15	281.59	5.0
A113	32.3/35.7	150.2±7	157.02	285.8±20	290.15	40.0
(100)	(29.2/42.1)	171.2±12	170.04	297.3±20	299.94	80
				159±20	157.41	5.0
A17S	51.7/42.1			165±15	170.49	58
(100)	(54.9/42.1)	90±10	95.41	186±15	193.90	153
		105±10	106.94	189±15	206.76	205
				120±20	129.62	5.0
A18S	58.2/42.1			128±15	140.36	58
(100)	(54.9/42.1)			145±20	152.21	91
		83±10	82.75	183±15	177.68	205
		100±10	102.42	220±10	231.27	4.2
A20S	38.8/38.9	119±10	124.25	228±10	251.43	78
(100)	(42.0/38.9)	190±20	190.61	279±10	312.73	300
				152±25	142.75	5.0
A21S	54.9/42.1			167±20	159.32	73
(100)	(Same)	83±10	67.62	186±15	174.92	137
		91±15	90.69	205±20	196.37	205
A69B	51.7/51.9					
(100)	(58.1/48.6)	80±15	78			120

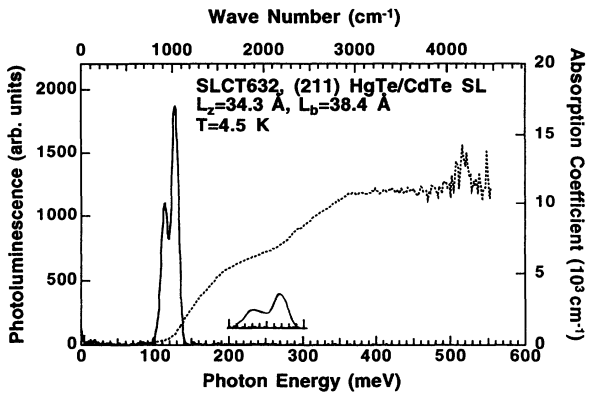

FIG. 4. The photoluminescence (solid curve) and the absorption spectra (dashed curve) of superlattice SLCT632 in the normal semiconducting regime with well width $L_z = 34.3$ Å and barrier width $L_b = 38.4$ Å at 4.5 K. The insertions show the magnified PL peaks near the $E1$-$L1$ band edge. The noise on the high-energy side was due to the low intensity of the light source in the spectral region.

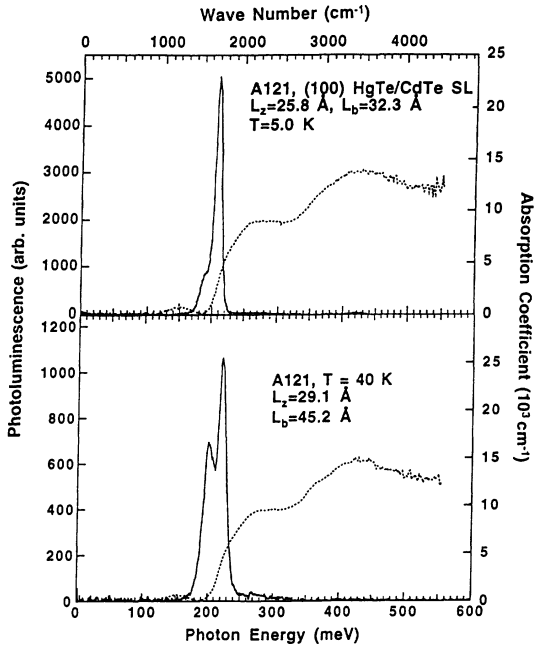

FIG. 5. The photoluminescence (solid curve) and the absorption spectra (dashed curve) of superlattice A121 in the normal semiconducting regime with well width $L_z = 25.8$ Å and barrier width $L_b = 32.3$ Å at 5 and 40 K.

energy peak was believed to be due to the $E1$-$L1$ exciton bound to the As acceptor.

Figure 5 shows the PL and absorption spectra of sample A121 at 5 and 40 K. The dominant PL peak at the $E1$-$H1$ band edge was due to the direct $E1$-$H1$ recombination. The lower-energy shoulder of the PL peak at 5 K developed into a separate peak (peak B) at 40 K as the intensity of the main peak decreased, while the intensity of the peak B remained almost unchanged. The peak position of peak B shifted to higher energy at a slower pace than the $E1$-$H1$ main peak. The intensity of peak B changed by about a factor of 3 when the laser spot was moved across the SL surface, indicating that this PL peak was associated with the local defect density in the SL.

TABLE II. The list of experimental and theoretical $E1$-$H1$ and $E1$-$L1$ gaps at various temperatures for superlattices in the normal semiconducting regime grown on the (211) crystal surface. The well and barrier thicknesses used in the calculation are also listed for each sample. The values of the thicknesses in the parentheses are the estimates from the growth parameters.

Sample (Orientation)	L_z(Å)/L_b(Å)	$E1$-$H1$ gap (meV) Experiment	$E1$-$H1$ gap (meV) Theory	$E1$-$L1$ gap (meV) Experiment	$E1$-$L1$ gap (meV) Theory	Temperature (K)
		129.6±2	125.49	261.4±5	271.14	5.0
SLCT617	36.9/63.5	141.3±3	137.14	262.7±20	280.30	40.0
(211)	(38.3/63.5)	154.8±3	152.13	277.9±20	292.10	85
		166.4±4	163.78	289.4±15	301.22	120
		130.7±2	132.30	261.6±5	269.01	5.0
SLCT632	34.3/38.4	140.1±3	143.76	269.4±20	277.76	40.0
(211)	(36.9/37.1)	152.8±4	156.20	276.9±20	287.27	78
		169.7±5	169.95	298.0±25	297.77	120
				175±20	168.04	5.0
SLCT619	48.8/39.7			175±30	176.78	40
(211)	(47.5/39.7)		95.41	185±20	186.76	80
		80±10	106.94	190±20	196.74	120
				149±25	180.62	5.0
A90B	50.1/62.2			175±25	191.30	40
(211)	(42.1/68.9)			190±25	203.16	80
		91.4±10	87.34	200±30	215.02	120
		154.6±10	146.88	289±20	295.49	5.0
A91B	34.3/62.2	162.3±10	158.49	297±20	304.59	40
(211)	(33.0/63.5)	173.7/±10	171.76	303±20	315.00	80
		183.4±10	185.03	315±20	325.40	120

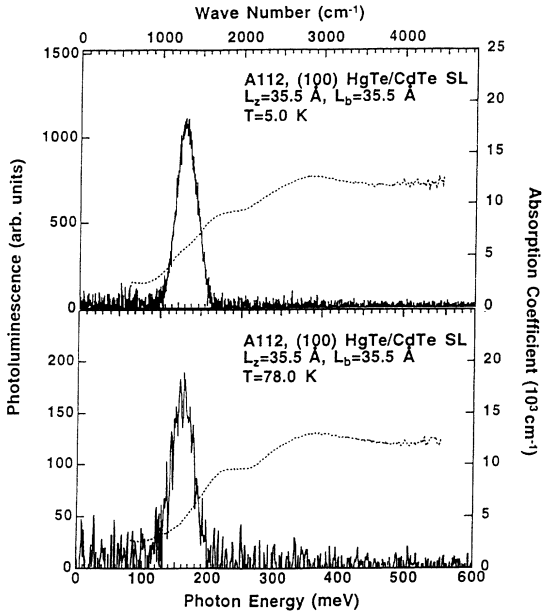

FIG. 6. The photoluminescence (solid curve) and the absorption spectra (dashed curve) of superlattice A112 in the normal semiconducting regime with well width $L_z = 35.5$ Å and barrier width $L_b = 35.5$ Å at 5 and 78 K.

The intensities of both peaks changed linearly with the laser pumping power.

Another type of PL peak was observed in sample A112 which was structurally inferior to the rest of the SL's, as is shown in Fig. 6. The peak position remained unchanged while the temperature was raised from 5 to 80 K. It was probably due to the radiative transition of electrons from deep donor level to deep acceptor levels caused by the structural defects.

5. *In-plane cyclotron motion of electrons and holes*

A single absorption line was observed in the ECR polarization for sample A90B. The absorption line at 4.5 K evolved into a new line at a higher magnetic field at higher temperatures, a manifestation of thermal redistribution of electrons on different energy levels in the SL. The points in Fig. 7 are the incident photon energy plotted as a function of the magnetic-field position of the absorption line at 4.5 and 40 K. The data points obtained at 40 K and higher temperatures (not shown in the figure) extrapolate to zero photon energy at zero magnetic field. The resonance was thus attributed to the cyclotron resonance of the $E1$ conduction subband electrons. The calculated electron transition energy at 40 K from the lowest Landau level as a function of the magnetic field, shown as the solid curve in Fig. 7, agrees well with the cyclotron resonance data points at 40 K. For the same photon energy the transitions from the higher Landau levels occurred at higher magnetic fields due to the strong nonparabolicity of the $E1$ subband. This explains why the experimental absorption line shifted to higher magnetic field at higher temperature, since more electrons were on higher Landau levels as the temperature was raised.

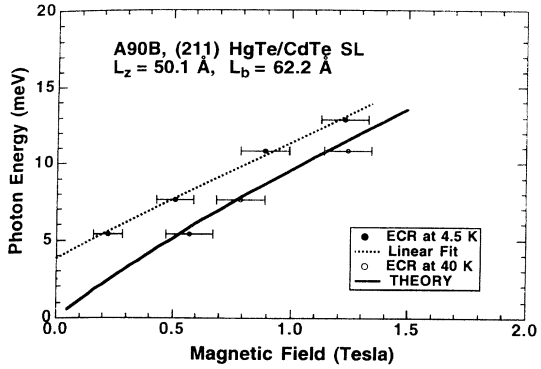

FIG. 7. The magnetic-field positions of the electron cyclotron resonance line versus the photon energy of the laser beam at 4.5 K (closed circle) and 40 K (open circle) for sample A90B. The dashed line is the linear least-squares fit to the data obtained at 4.5 K and the solid curve is the calculated energy of the allowed optical transition from the lowest Landau level of the $E1$ subband to the higher level as a function of the magnetic field.

The same ECR was observed in (211)-oriented SLCT619 and (100)-oriented A69A SL's. The experimental in-plane effective mass of the $E1$ subband for SLCT619 was $(0.010\pm0.002)m_0$, which agrees well with the calculated mass of $0.0096m_0$, and the measured in-plane mass for A69A was 0.011 ± 0.002, as compared with the theoretical value of 0.013.

The magnetotransmission spectra of sample SLCT632 show in-plane hole cyclotron resonance at 4.5 K. This is consistent with the Hall results that the SL is p type with a constant hole concentration of about 1.0×10^{17} cm^{-3} at temperatures below 140 K and provides additional direct evidence that the SL was, indeed, modulation doped with holes. The in-plane effective mass obtained from the experimental data is $(0.0185\pm0.0035)m_0$. The theoretical value of the in-plane hole mass is $0.022m_0$, which agrees fairly well with the experimental one.

6. *Donor level*

The dashed line in Fig. 7 represents a linear least-squares fit to the experimental points at 4.5 K. It intercepts the energy axis at 3.8 ± 1.0 meV, indicating that the absorption line of sample A90B at 4.5 K was probably due to the $1S$-to-$2P$ transition of a shallow donor level introduced by either impurities or native defects. From the slope of the line it was found that the effective mass of the bound electron was $(0.0147\pm0.001)m_0$, assuming a simple hydrogenlike shallow donor model. It agrees fairly well with the calculated $E1$ subband in-plane electron mass of $0.011m_0$ at 4.5 K. A similar $1S$-to-$2P$ transition was observed in sample A91B. The linear least-squares fit of the data points yielded a donor $1S$-to-$2P$ energy of 5 ± 2 meV at zero field and an electron effective mass of $(0.020\pm0.005)m_0$, which is in good agreement with the $E1$ subband in-plane mass of $0.02m_0$ predicted by theory. No attempt was made to fit the ionization energy of the donor level using the effective mass because of the possible chemical shift.

7. *Cyclotron motion in the Voigt geometry*

The cyclotron movement of carriers perpendicular to the layer plane was observed in sample SLCT619. Shown in Fig. 8 is the magnetotransmission spectrum of SLCT619 at 4.5 K with the magnetic field parallel to the layer plane (Voigt geometry). This was the first time the cyclotron motion of carriers was observed in an open-gap HgTe/CdTe SL, since all the previous observations were made in SL's with either zero gaps[18] or inverted-band gaps.[13] The plot of the magnetic-field position of the absorption line versus photon energy forms a straight line which extrapolates to zero energy at zero field. The effective mass of the carriers obtained from the slope of the straight line was $(0.031\pm0.005)m_0$. Following the example in Ref. 13, we proceeded to estimate the Voigt-geometry effective mass by theory. The calculated in-plane and perpendicular masses for the conduction subband electrons were $m_{\parallel}=0.0096m_0$ and $m_{\perp}=0.287m_0$, respectively, and the mass of the cyclotron motion in the Voigt geometry was therefore $m_V=0.052m_0$. The discrepancy was probably due to the simple model and the lack of precise information, such as the x value of the $Hg_{1-x}Cd_xTe$ alloy, of the barrier layers.

B. Semimetallic regime

Extremely light masses of both electrons and holes were found in sample A122B with well width corresponding to the semimetallic regime by using the far-infrared magneto-optical spectroscopy. The electron and hole mobilities found from Hall data were both 3×10^4 cm^2/Vs at 4.2 V, which was consistent with the light masses of the carriers.

The effective masses of electrons m_e and holes m_h in a SL in the semimetallic regime are strongly k_z dependent. At the point $k_z=k_c$ where the $E1$ and the $H1$ subbands cross each other [see Fig. 1(b)] the masses of electrons and holes are very small, while at $k_z=0$ at $k_z=\pi/d$ (d is the period of the SL), where the $E1$ and the $H1$ subbands split apart, the masses can be ten times larger. At low temperatures, most of the free electrons are on the low-energy portion of the conduction subband, which is the portion of the $H1$ subband from $k_z=0$ to $k_z=k_c$, while most of the free holes are on the high-energy portion of the valence subband, which is the rest of the $H1$ subband. An electron on the $H1$ conduction subband can stay at any of the $k_z<k_c$ states with a mass of $m_e(k_z)$, because the $H1$ subband is almost flat along the k_z direction. As a result, the effective masses of the electrons participating in the cyclotron resonance range from $m_e(0)$ and $m_e(k_c)$ and the resonant line will therefore be significantly broadened. Likewise, the effective masses of the holes range from $m_h(k_c)$ to $m_h(\pi/d)$ and the hole cyclotron resonance line will also be broadened.

Figure 9 shows the cyclotron resonance of electrons [Fig. 9(a)] and holes [Fig. 9(b)] of A122B taken at the wavelength of 118.9 μm (10.4 meV) at 4.5 K in the Faraday geometry. The electron cyclotron resonance was distinguished from that of the holes by comparing the sense of the polarization of the laser beam with the direction of the magnetic field. From the transition energy between the $H2$ subband and the $E2$ subband obtained from the IR absorption spectra of the SL and the growth parameters, it was determined that the well and barrier thicknesses of the SL were $L_z=74.3$ Å and $L_b=25.9$ Å. The SL was therefore in the semimetallic regime at 4.5 K. Theoretical analysis showed that the $E1$ subband crossed the $H1$ subband at $k_c=0.33\pi/d$. The electron and hole concentrations obtained from the mobility spectrum

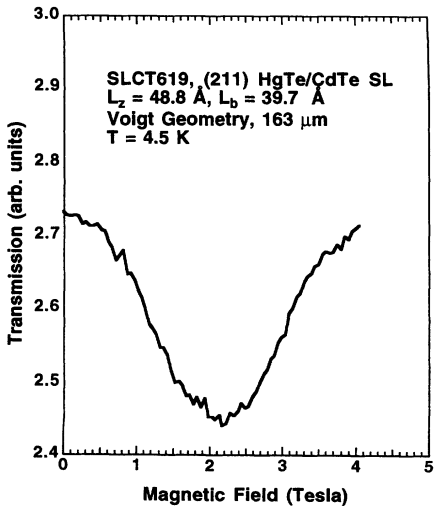

FIG. 8. The magnetotransmission spectrum of superlattice SLCT619 in the Voigt geometry in which the magnetic field was parallel to the layers of the superlattice. The wavelength of the incident laser beam was 163 μm.

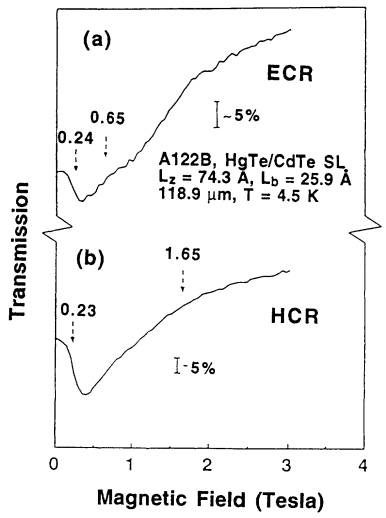

FIG. 9. Far-infrared magnetotransmission spectra of superlattice A122B in the semimetallic regime with well width $L_z=74.3$ Å and barrier width $L_b=25.9$ Å in (a) electron cyclotron resonance polarization and (b) hole cyclotron resonance polarization at 4.5 K and 118.9 μm. Both the magnetic field and the laser beam are perpendicular to the superlattice layers. The arrows indicate the theoretical maximum (dashed) and minimum (solid) magnetic fields at which the energies of the optical transitions between Landau levels for the electrons or the holes at different K_z are equal to the incident photon energy.

analysis of the Hall data were $n=2.7\times10^{15}$ cm^{-3} and $p=2.8\times10^{15}$ cm^{-3} at 4.2 K. Therefore, only the lowest Landau level of the conduction subband was occupied by the electrons and the highest Landau level of the valence subband was occupied by the holes at magnetic fields exceeding 0.1 T. The energies of the optical transitions from these Landau levels to the higher-order levels, following the selection rules that the Landau level number changes by $+1$ for the electron cyclotron resonance and by -1 for the hole cyclotron resonance, were calculated and were found to be strongly k_z dependent. The dashed arrows in Fig. 9(a) point out the values of the magnetic fields at which the electron transition energy is equal to the photon energy of the incident laser beam at $k_z=0$ and $0.33\pi/d$, respectively. Similarly, the dashed arrows in Fig. 9(b) indicate the fields at which the hole transition energy is equal to the photon energy at $k_z=\pi/d$ and $k_z=0.33\pi/d$. In both the ECR and the HCR cases, the observed resonant lines fall within the theoretical maximum and minimum magnetic fields indicated by the arrows, consistent with the theory.

C. Inverted-band regime

All nine inverted-band SL's were grown on (100) CdTe or CdZnTe substrates, and were n type with an electron concentration of about 5×10^{16} cm^{-3}. The samples were actually MQW's since the barrier thicknesses of them were larger than 45 Å. Theoretical calculation showed that in an inverted-band MQW, the $H1$ subband was the first *conduction* subband, while the $E1$ subband was the first *valence* subband. The second conduction and valence subbands were the $E2$ subband and the $H2$ subband, respectively. The energy gap between the $H1$ and $E1$ subbands was of the order of 20 meV, while the gap between $E2$ and $H2$ was within the IR spectral range.

Figure 10 shows the absorption spectra of three MQW's at 4.5 K. A large absorption edge appeared at photon energies 270, 180, and 110 meV for samples A67A, A58B, and A27A, respectively. The well and barrier thicknesses listed in the figure are the nominal values estimated from the growth parameters. The edge shifted to lower photon energy with thicker well, in agreement with the fact that there was less and less quantum confinement. The sharp absorption spike for sample A27A indicated that the sample was of excellent optical quality. Similar sharp spikes were observed in other inverted-band SL's. The absorption was non-zero in the entire spectrum region, indicating that the $E1$-$H1$ gap of these SL's was indeed very small (<50 meV). Theoretical analysis showed that the $H2\rightarrow E2$ transition was a strong transition and the transition energy was close to the energy position of the observed absorption edge. The nonparabolicity of the $H2$ subband and the k_x-dependent transition probability resulted in the sharp peak structure, where k_x is the in-plane component of the electron wave vector. All the absorption structures shifted to higher energy as the temperature was raised, and the peak structure reduced to steplike edge at room temperature.

Figure 11 shows the far-infrared magnetotransmission

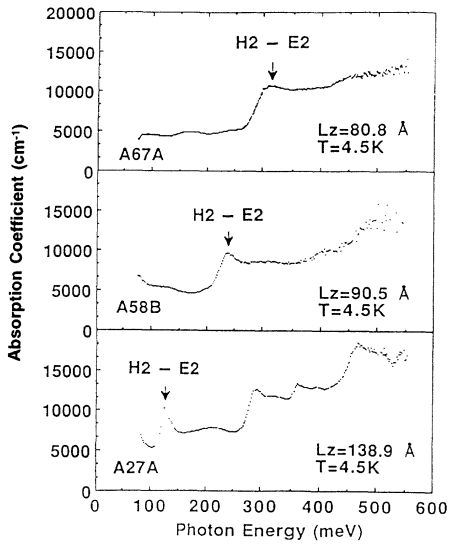

FIG. 10. The infrared-absorption spectra of three inverted-band superlattices at $T=4.5$ K. The absorption peak due to the $H2$-to-$E2$ transition is shown. The well widths estimated from the growth parameters for the three samples are $L_z=80.8$ Å for sample A67A, $L_z=90.5$ Å for A58B, and $L_z=138.9$ Å for A27A, respectively.

spectra of the same samples shown in Fig. 10. The spectra were taken in the ECR polarization at 4.5 K, and at a fixed far-infrared wavelength of 118.9 μm. Two strong absorption lines, labeled A and B, respectively, were clearly observed in these samples. In other samples, one strong absorption line was observed in the ECR polarization. The absorption lines were due to the cyclotron resonance of the electrons on the $H1$ subband. The fact that

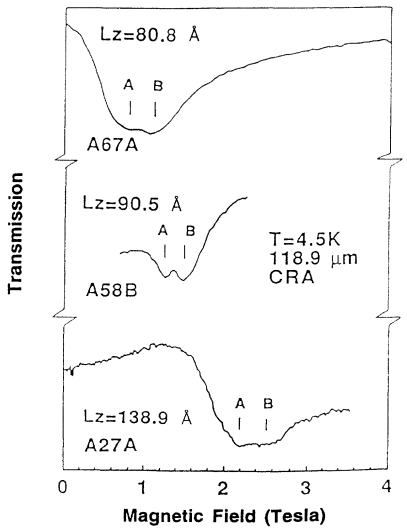

FIG. 11. The far-infrared magnetotransmission spectra of the same samples as presented in Fig. 10 at $T=4.5$ K and at a fixed wavelength of 118.9 μm. The far-infrared laser beam is circularly polarized in the electron-cyclotron-resonance active sense, and both the magnetic field and the laser beam are perpendicular to the superlattice layer plane. The two absorption lines are labeled A and B.

there were two absorption lines indicates that the conduction subband $H1$ was strongly nonparabolic. The magnetic-field positions of both absorption lines moved to *higher* fields for SL's with wider wells. This implies that the in-plane electron mass *increased* with the increase of the well width, since the in-plane electron effective mass is directly proportional to the magnetic-field position of the cyclotron resonance absorption line at a given photon energy.

To further prove that the effective mass indeed increases with the well width, another way to determine the well widths besides estimation from the growth parameters is required. This was provided by the $E2$-$H2$ gap energy measured from the IR absorption spectra of the same sample, since for a given well width, there is only one value of the $E2$-$H2$ gap energy. In Figs. 12(a) and 12(b) the magnetic-field positions of lines A and B at a fixed wavelength of 118.9 μm of each SL are plotted as a function of its measured $E2$-$H2$ gap energy (points), respectively. It is seen that the magnetic-field positions of the absorption lines increase as the $E2$-$H2$ gap energy decreases. The decrease in energy of the $E2$-$H2$ gap indicates the increase of the well width. It is therefore evident that the in-plane electron effective mass indeed *increases* as the well width *increases*. Such a relation for the MQW's in the inverted-band regime is distinctively different from that for the SL's and MQW's in the normal regime, where the effective mass *decreases* with the *increase* of the well width. This is because the effective mass is roughly proportional to the $E1$-$H1$ gap energy. For SL's in the normal semiconducting regime, the $E1$-$H1$ gap decreases as the well width increases. The effective mass therefore decreases. For SL's in the inverted-band regime, the $E1$ subband moves further away from the $H1$ subband after they cross each other as the well width increases. The effective mass thus increases with the increase of the well width. Such a relation is unique only for the SL's and MQW's in the inverted-band regime.

The solid lines in Figs. 12(a) and 12(b) are the theoretical results using VBO=550 meV at 4.5 K, while the dashed lines are the ones using VBO=400 meV. Line A is attributed to the electronic transition from the lowest Landau level (-2) to the second lowest level (-1), while line B is attributed to the transition from the (-1) level to the (0) level, since at a concentration of 5×10^{16} cm^{-3} the (-1) level was also partially occupied. The theoretical curves using VBO=550 meV fit much better than the ones using VBO=400 meV. More results are shown in Figs. 13 and 14 for wavelengths 96.5 and 163 μm, respectively, and the theoretical results also agree well with the experimental ones at these two wavelengths.

The theoretical results using VBO=40 meV as suggested in Refs. 10–12, however, contradict qualitatively with the experimental results shown in Figs. 12–14. In fact,

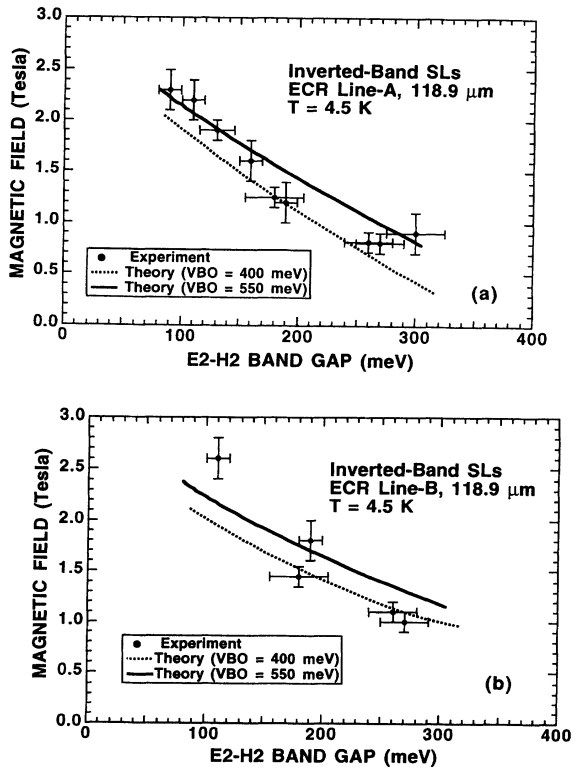

FIG. 12. The magnetic-field position of lines A and B of each sample at 118.9 μm as a function of its $E2$-$H2$ band gap measured from the absorption spectra (points). The solid and the dashed curves are the theoretical results using VBO=550 and 400 meV, respectively.

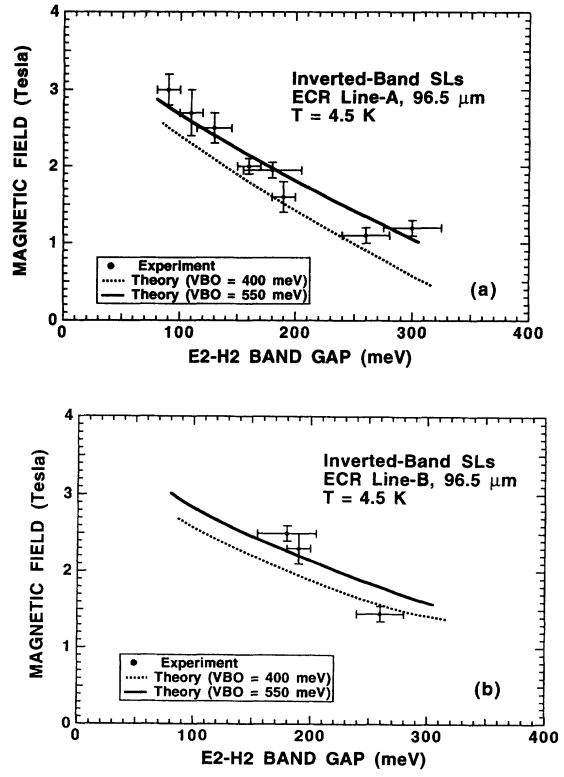

FIG. 13. The magnetic-field position of lines A and B of each sample at 96.5 μm as a function of its $E2$-$H2$ band gap measured from the absorption spectra (points). The solid and the dashed curves are the theoretical results using VBO=550 and 400 meV, respectively.

none of the SL's were predicted to be in the inverted-band regime when VBO=40 meV was used. As a result, the in-plane electron effective mass of the SL's decreased with the increase of the well width, in qualitative disagreement with the experimental results.

We now proceed to compare the theory with the rest of the experimental results. Figure 15 shows the comparison between the experimental $E2$-$H2$ gap energy (points) and the theoretical ones (solid line) at 4.5 K for the nine SL's with VBO=550 meV. The estimated value of the well width from the growth parameters for each sample was used for the experimental points. It is seen that the experimental points do not fall into a smooth line, an indication that the estimation of the well width was not very accurate. A correction of two to eight ML's for the well width was needed in order for the experimental band gaps to fall on the theoretical curve. It is quite possible that the nominal well widths were all underestimated from the growth parameters because the wells were all fairly thick.

Figure 16 shows the experimental $E2$-$H2$ gap energy as a function of temperature (points) for sample A57B and the theoretical fit using VBO=550 meV (solid line) and VBO=450 meV (dashed line). The well width of the SL was adjusted according to Fig. 15 so that the experimental gap energy fits the theoretical one at 4.5 K for VBO=550 meV. It is seen that both curves agree well with the experimental results, and the temperature

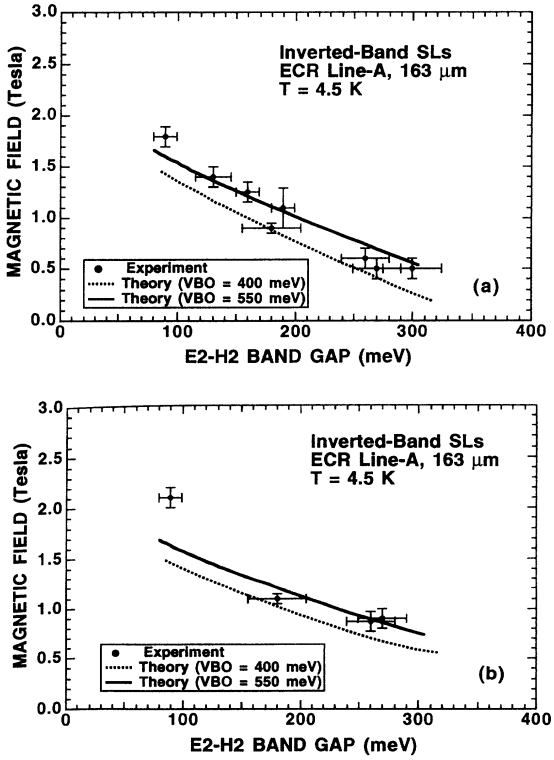

FIG. 14. The magnetic-field position of lines A and B of each sample at 163 μm as a function of its $E2$-$H2$ band gap measured from the absorption spectra (points). The solid and the dashed curves are the theoretical results using VBO=550 and 400 meV, respectively.

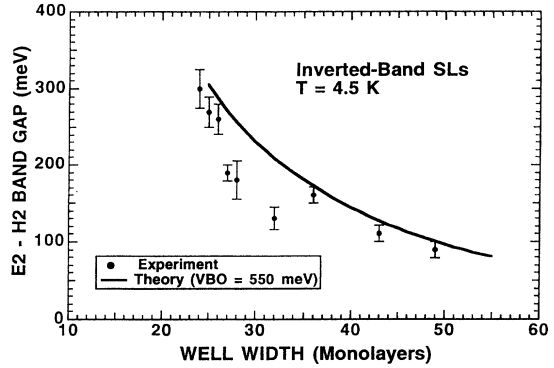

FIG. 15. The experimental $E2$-$H2$ band gap as a function of the well width in units of monolayers (points) at 4.5 K. Each monolayer is 3.231 Å thick. The solid curve is the theoretical band gap using VBO=550 meV.

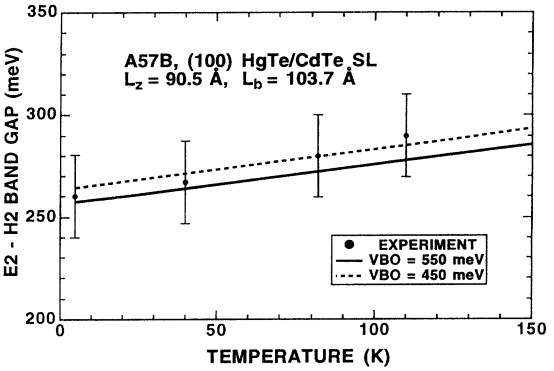

FIG. 16. The experimental $E2$-$H2$ band gap (points) versus temperature for sample A57B and the theoretical transition energy using VBO=550 meV (solid line) and VBO=450 meV (dashed line). The layer thicknesses used in the calculation were L_z=90.5 Å for the wells and L_b=103.7 Å for the barriers, respectively.

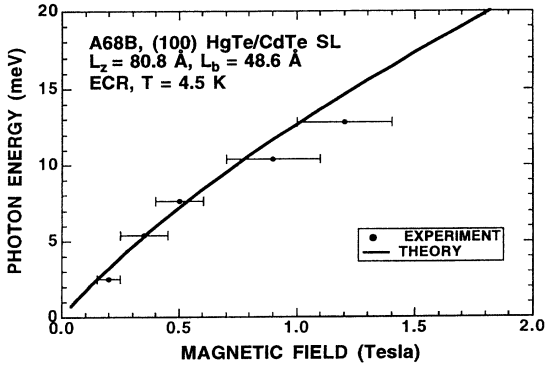

FIG. 17. The magnetic-field positions of the electron cyclotron resonance line versus the photon energy of the laser beam at 4.5 K (points) for sample A68B. The solid curve is the calculated energy of the allowed optical transition from the lowest Landau level of the $E1$ subband to the higher level as a function of the magnetic field. The layer thicknesses used in the calculation were L_z=80.8 Å for the wells and L_b=48.6 Å for the barriers, respectively.

dependence of VBO can be neither confirmed nor rejected because of the large error margins of the measured gaps.

Figure 17 shows the magnetic-field positions of line A for one of the nine samples, A68B, at several fixed incident photon energies (points) at 4.5 K. The curve is the calculated transition energies between the Landau levels (-2) and (-1) as a function of the magnetic field, using the same well width shown in the figure. Good agreement is found between the experimental and the theoretical results.

V. DISCUSSION

We have demonstrated for the first time that all the major subband features of the HgTe/CdTe SL's predicted by the six-band $\mathbf{k}\cdot\mathbf{p}$ model with a single value of 550 meV for the valence-band offset agree quantitatively with the experimental results obtained from the SL's with a wide range of well and barrier thicknesses and over a wide range of temperatures. This includes the $E1$-$H1$ band gap, the $E1$-$L1$ band gap, the $E2$-$H2$ band gap, the in-plane effective masses of electrons and holes, and the Voigt-geometry effective mass of electrons. It is essential to compare at least two major subband features with experiments before a conclusion on the value of VBO is drawn. This is because ambiguities may occur in determining VBO if only one subband feature is measured. For example, with certain well width the in-plane electron mass predicted by using VBO=400 meV is the same as the one predicted by using VBO=40 meV,[11] the difference being that the SL is either in the inverted-band regime for VBO=400 meV or in the normal semiconducting regime for VBO=40 meV. Such ambiguities are not present in this work because the subband gaps of the SL's have also been measured.

For the SL's in the normal semiconducting regime, the two major subband features which can be measured with good precision are the $E1$-$H1$ band gap and the in-plane mass of either electrons or holes. The measured $E1$-$L1$ gap and the subsequent $H1$-$L1$ gap of the order of 100 meV provide additional information and put a lower limit on the VBO, i.e., the value of VBO should be larger than the measured $H1$-$L1$ gap, although the measured gap is usually associated with a larger error than the $E1$-$H1$ gap. Analysis of the $E1$-$H1$ gap and the in-plane mass of the SL's in the normal regime yields a VBO of 500 ± 100 meV. The uncertainty of ±100 meV for VBO is mainly due to the errors in determining the HgTe and CdTe layer thicknesses. Using TEM, it is quite straightforward to determine the layer thicknesses. Unfortunately, due to limited resources, only a small number of samples were examined with TEM. The layer thicknesses of the rest of the samples were determined by combining the growth parameters, the x-ray rocking curves, and the total thickness measurements, and using the TEM data of the few samples as references. The errors of the layer thicknesses thus determined are ±2 ML's for the (100)-oriented SL's and ±4 ML's for the (211)-oriented SL's.

The calculated band gaps are very sensitive to the well width but are not so to the value of VBO. For example, an $E1$-$H1$ gap of 132.3 meV is obtained for SLCT632, which has a measured band gap of 130.7 ± 2 meV at 5 K, when VBO=550 meV is used along with $L_z=34.4$ Å and $L_b=38.4$ Å. Increasing L_z by 1 ML to 36.9 Å while decreasing L_b by 1 ML to 37.1 Å put the band gap to 133.44 meV when VBO=400 meV is used. To obtain the same band gap, a 1-ML change of well width then requires a change of 150 meV of the value of VBO. The changes in band gap with the temperature are also almost the same for both sets of parameters. This is common for all the other SL's in the normal regime. Overall, the effective masses of all the samples calculated by using VBO=550 meV fit the measured values better than the ones using VBO=400 meV, while for the $E1$-$L1$ gap, the comparison between the two values of VBO is inconclusive. The results of the SL's in the normal regime therefore tend to support VBO=550 meV rather than VBO=400 meV, but the evidence is still inconclusive. Theoretical results obtained using VBO=40 meV, however, fit the experimental results poorly.

The deciding evidence that supports VBO=550 meV rather than 400 meV is provided by the analysis of the $E2$-$H2$ band gap and the electron mass of the MQW's in the inverted-band regime. The calculated $E2$-$H2$ gap versus the electron mass using VBO=550 meV clearly agrees much better than the one using VBO=400 meV, as is shown in Figs. 12–14. The estimated uncertainty for VBO is ±50 meV. Taking into account the analysis in Secs. IV A 1–IV A 3 where the temperature dependence of the VBO was discussed, we are able to conclude that the value of VBO is 550 ± 50 meV at 4.5 K and reduces, probably linearly, to 500 ± 50 meV at 120 K.

VI. CONCLUSION

HgTe/CdTe superlattices in the three principal regimes, namely, the normal semiconducting regime, the semimetallic regime, and the inverted-band regime, have been studied systematically. Photoluminescence due to the direct recombination between the $E1$-$H1$ electron-hole pairs and between the $E1$-$L1$ electron-hole pairs, as well as the impurity- and (or) defect-related recombination, have been observed in the SL's in the normal semiconducting regime. The $E1$-$H1$ and the $E1$-$L1$ band gaps have been measured from the main PL peaks and from the absorption edges at different temperatures. The in-plane cyclotron motion of electrons and holes, as well as the cyclotron motion of electrons perpendicular to the layers, have been observed in the FIR magnetotransmission spectra of the SL's in the normal semiconducting regime. Cyclotron motion of both electrons and holes with extremely light effective mass have been observed in a SL in the semimetallic regime. The inverted-band HgTe/CdTe superlattices have been studied in the IR transmission and far-infrared magnetotransmission experiments. The in-plane cyclotron resonance of the conduction-band electrons has been observed and the effective mass of the electrons on the inverted first conduction subband $H1$ has been directly measured. The effective mass *increased* with the *increase* of the well width, indicating that these SL's are indeed inverted-band SL's. The $E2$-$H2$ band gap obtained from the IR

transmission spectra decreased as the well width was increased, in agreement with the fact that there was less and less quantum confinement as the well width increases. With a single value of 550 meV for the valence-band offset, the six-band $\mathbf{k}\cdot\mathbf{p}$ model correctly predicted all the experimental results. These include (i) the $E1$-$H1$ and the $E1$-$L1$ band gaps of the SL's in the normal regime over the temperature range from 5 to 150 K; (ii) the in-plane effective masses of the electrons and holes, as well as the Voigt-geometry effective mass of electrons, for the SL's in the normal semiconducting regime at 5 K; (iii) the in-plane electron and hole masses in a SL in the semimetallic regime at 5 K; (iv) the $E2$-$H2$ band gaps of the SL's in the inverted-band regime in the temperature range from 5 to 150 K; and (v) the electron in-plane masses of the SL's in the inverted-band regime at 5 K. The VBO has been found to decrease slowly with the increase of temperature. The best value of VBO to fit the experimental results is 550±50 meV at 5 K and it reduces, probably linearly, to 500±50 meV at 120 K.

ACKNOWLEDGMENTS

This work was supported by Ms. Lynn Brown of the Materials Directorate, Wright Laboratory, Wright Patterson Air Force Base, under Contract No. F33615-90-C-5922, and by the National Science Foundation through the computer resource allocation at the Cornell University IBM Supercomputer Center.

*Present address: Department of Physics, Hong Kong University of Science and Technology, Clear Water Bay, Kowloon, Hong Kong.

[1]J. N. Schulman and T. C. McGill, Appl. Phys. Lett. **34**, 663 (1979).
[2]P. M. Hui, H. Enrenreich, and N. F. Johnson, J. Vac. Sci. Technol. A **7**, 424 (1989).
[3]Z. Yang, Z. Yu, Y. Lansari, J. W. Cook, Jr., and J. F. Schetzina, J. Vac. Sci. Technol. B **9**, 1799 (1991).
[4]S. R. Hetzler, J. P. Baukus, A. T. Hunter, J. P. Faurie, P. P. Chow, and T. C. McGill, Appl. Phys. Lett. **47**, 260 (1985).
[5]J. P. Baukus, A. T. Hunter, O. J. Marsh, C. E. Jones, G. Y. Wu, S. R. Hetzler, T. C. McGill, and J. P. Faurie, J. Vac. Sci. Technol. A **4**, 2110 (1986).
[6]Y. Lansari, J. W. Han, S. Hwang, L. S. Kum, J. W. Cook, Jr., and J. F. Schetzina, J. Vac. Sci. Technol. A **7**, 241 (1989).
[7]N. F. Johnson and H. Ehrenreich, Surf. Sci. **228**, 197 (1990).
[8]Z. Yang, Y. Lansari, J. W. Cook, Jr., and J. F. Schetzina (unpublished).
[9]C. L. Cesar, M. H. Islam, R. D. Feldman, R. F. Austin, D. S. Chemla, L. C. West, and A. E. DiGiovanni, Appl. Phys. Lett. **56**, 283 (1990).
[10]J. M. Berroir, Y. Guldner, J. P. Vieren, and M. Voos, Phys. Rev. B **34**, 891 (1986).
[11]J. B. Choi, L. Ghenim, R. Mani, H. D. Drew, K. H. Yoo, and J. T. Cheung, Phys. Rev. B **41**, 10 872 (1990).
[12]Z. Yang, M. Dobrowolska, H. Luo, J. K. Furdyna, and J. T. Cheung, Phys. Rev. B **38**, 3409 (1988).
[13]J. M. Berroir, Y. Guldner, J. P. Vieren, M. Voos, X. Chu, and J. P. Faurie, Phys. Rev. Lett. **62**, 2024 (1989).
[14]S. P. Kowalczyk, J. T. Cheung, E. A. Kraut, and R. W. Grant, Phys. Rev. Lett. **56**, 1605 (1986).
[15]D. L. Smith and C. Mailhiot, Phys. Rev. B **33**, 8345 (1986).
[16]L. R. Ram-Mohan, K. H. Yoo, and R. L. Aggarwal, Phys. Rev. B **38**, 6151 (1988).
[17]D. G. Seiler, J. R. Lowney, C. L. Littler, and M. R. Loloee, J. Vac. Sci. Technol. A **8**, 1237 (1990).
[18]R. J. Wagner, J. M. Perez, J. R. Meyer, J. W. Han, J. W. Cook, Jr., and J. F. Schetzina, J. Vac. Sci. Technol. A **7**, 411 (1989).